

Real-Time Visualization of Diffusion-Controlled Nanowire Growth in Solution

Shengrong Ye,^{1,†} Zuofeng Chen,^{1,†,‡} Yoon-Cheol Ha,^{1,†,§} and Benjamin J. Wiley^{*,†}

[†]Department of Chemistry, Duke University, Durham, North Carolina 27708, United States

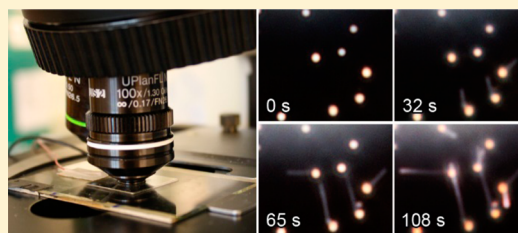
[‡]Department of Chemistry, Tongji University, Shanghai 200092, China

[§]Creative and Fundamental Research Division, Korea Electrotechnology Research Institute, Changwon 642-120, Republic of Korea

S Supporting Information

ABSTRACT: This Letter shows that copper nanowires grow through the diffusion-controlled reduction of dihydroxycopper(I), $\text{Cu}(\text{OH})_2^-$. A combination of potentiostatic coulometry, UV–visible spectroscopy, and thermodynamic calculations was used to determine the species adding to growing Cu nanowires is $\text{Cu}(\text{OH})_2^-$. Cyclic voltammetry was then used to measure the diffusion coefficient of $\text{Cu}(\text{OH})_2^-$ in the reaction solution. Given the diameter of a Cu nanowire and the diffusion coefficient of $\text{Cu}(\text{OH})_2^-$, we calculated the dependence of the diffusion-limited growth rate on the concentration of copper ions to be $26 \text{ nm s}^{-1} \text{ mM}^{-1}$. Independent measurements of the nanowire growth rate with dark-field optical microscopy yielded $24 \text{ nm s}^{-1} \text{ mM}^{-1}$ for the growth rate dependence on the concentration of copper. Dependence of the nanowire growth rate on temperature yielded a low activation energy of 11.5 kJ mol^{-1} , consistent with diffusion-limited growth.

KEYWORDS: anisotropic assembly, growth mechanism, copper nanowires, diffusion control, real time visualization



Self-assembly is the spontaneous organization of components such as atoms and molecules into patterns or structures (e.g., crystals) without human intervention.^{1,2} In the past decade, the number of syntheses available that enable control over the anisotropic self-assembly of atoms into nanostructures has increased from less than a dozen to thousands.^{3–9} The ability to make and use anisotropic nanostructures has advanced tremendously, but the degree to which the growth process is understood depends upon the synthetic methodology. For nanowire growth in the vapor phase, it is generally recognized that semiconductor nanowires grow via a process in which material in the vapor phase is incorporated into a growing nanowire via nanoparticle catalysts.^{10–12} For self-assembly in the liquid phase, CdTe nanowires, iron oxyhydroxide nanowires, and PbSe nanorods have been shown to grow through the oriented attachment of smaller spherical nanoparticles.^{13–15} Bi_2S_3 nanowires have recently been shown to exhibit polymer-like nanowire growth kinetics.¹⁶ In contrast, for metal nanowires, it is not clear whether the species adding to the nanostructure consists of metal ions, reduced metal atoms, or metal clusters. In addition, it is not clear what mechanistic step limits the rate of nanostructure growth.

Metal nanowires have the potential to be a low cost replacement for the transparent conductor, indium tin oxide (ITO), in touch screens, flat-panel displays, thin-film solar cells, and organic light emitting diodes.^{17–20} Improving the properties and cost of nanowire-based transparent electrodes requires greater control over the structure and yield of nanowires in solution phase syntheses, which in turn motivates mechanistic

studies of nanowire growth in solution. However, as the growth of metal nanowires has generally been difficult to observe in real time, there is as yet very little quantitative analysis of nanowire growth kinetics in solution, let alone a clear relationship between the growth kinetics and nanostructure morphology.^{11,21–25} The recent development of *in situ* transmission electron microscopy (TEM) and transmission X-ray microscopy (TXM) has enabled the real time visualization of spherical nanoparticle and nanorod growth in a liquid environment, semiconductor nanowire growth in the vapor phase, as well as the galvanic replacement reaction between Ag nanowires and HAuCl_4 .^{11,12,21,24,26–33} TEM or TXM-based visualization has yet to be applied to the solution-phase growth of nanowires, perhaps due to the lack of temperature control and the high cost of the current technology.

Cu nanowires synthesized through the ethylenediamine-(EDA-) mediated approach have previously been shown to grow along the [110] direction with a 5-fold twinned crystal structure.^{34–36} This growth direction and crystal structure is the same as for Ag nanowires grown with a polyol synthesis using polyvinylpyrrolidone (PVP) as a capping agent.³⁷ Similar to the case of Ag nanowires and PVP, it has been hypothesized that EDA preferentially binds to the higher surface energy {100} facets that make up the sides of the wire, leaving the lower energy {111} facets on the ends of the nanowire open to

Received: May 12, 2014

Revised: June 30, 2014

Published: July 23, 2014

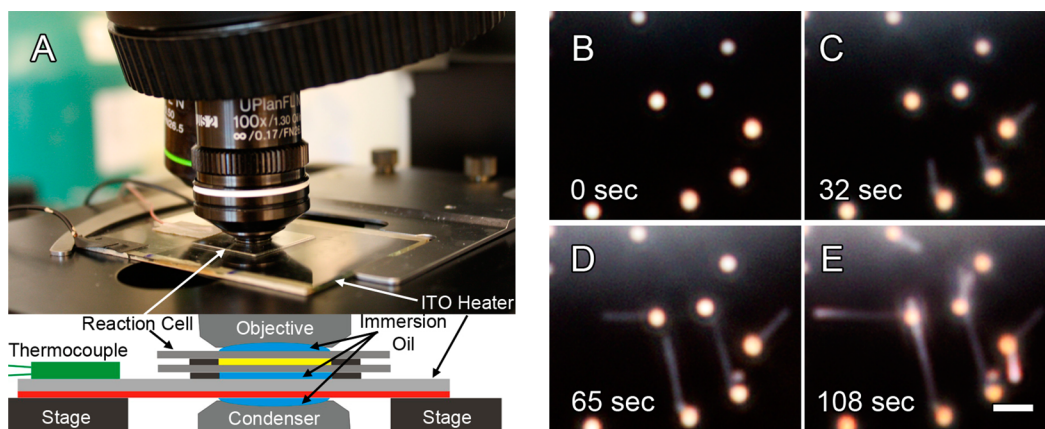


Figure 1. (A) Camera image and schematic cross-sectional view of the reaction cell with the dark field optical microscope. Real time growth of Cu nanowires recorded at (B) 0, (C) 32, (D) 65, and (E) 108 s. Scale bar is 2 μm .

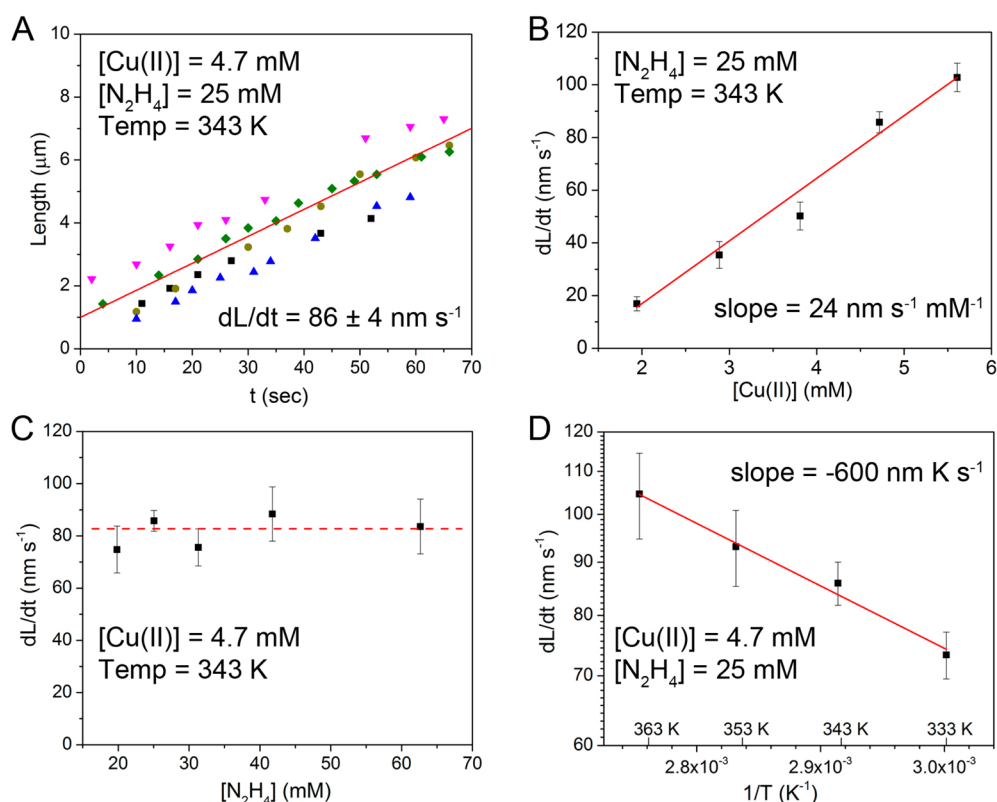


Figure 2. (A) Plot of length versus time for five Cu nanowires. Dependence of the growth rate on the (B) $[\text{Cu(II)}]$, (C) $[\text{N}_2\text{H}_4]$, and (D) temperature. Each data point and error bar in parts B–D represents the average and standard deviation of ten measurements.

atomic addition. Indeed, it has previously been shown that increasing the concentration of EDA in the Cu nanowire synthesis decreases the rate of addition of Cu to the ends of the nanowires.³⁸ However, it was not clear what species was adding to the nanowire or what mechanical step limited its rate of growth.

Here we introduce a growth model derived from real time observation of Cu nanowire growth in solution with dark field optical microscopy (DFOM).³⁸ By enabling the measurement of the axial growth rate of nanowires in real time, DFOM provides a way to probe the reaction mechanism under a variety of conditions quickly, and at relatively low cost. By using DFOM to observe the growth rates of Cu nanowires grown at various reaction temperatures, concentrations of $\text{Cu}(\text{NO}_3)_2$,

and concentrations of N_2H_4 , we determined that Cu nanowires grow through the diffusion limited reduction of $\text{Cu}(\text{OH})_2^-$.

The initial formation of Cu seed particles and subsequent nanowire growth can be visualized in a reaction cell situated in the viewing plane of a dark field optical microscope (see Figure 1A, experimental details are given in the Supporting Information). The reaction solution is made by mixing NaOH , $\text{Cu}(\text{NO}_3)_2$, EDA, and N_2H_4 in water at room temperature. A typical nanowire growth process (see Movie S1, Supporting Information) at 343 K was recorded at rate of 1 frame per second. Four frames extracted at 0, 32, 65, and 108 s are shown in Figure 1B–E. Here, 0 s is chosen as the last frame in which no nanowire is visible. The reaction temperature was monitored by a thermocouple situated next to the cell; this

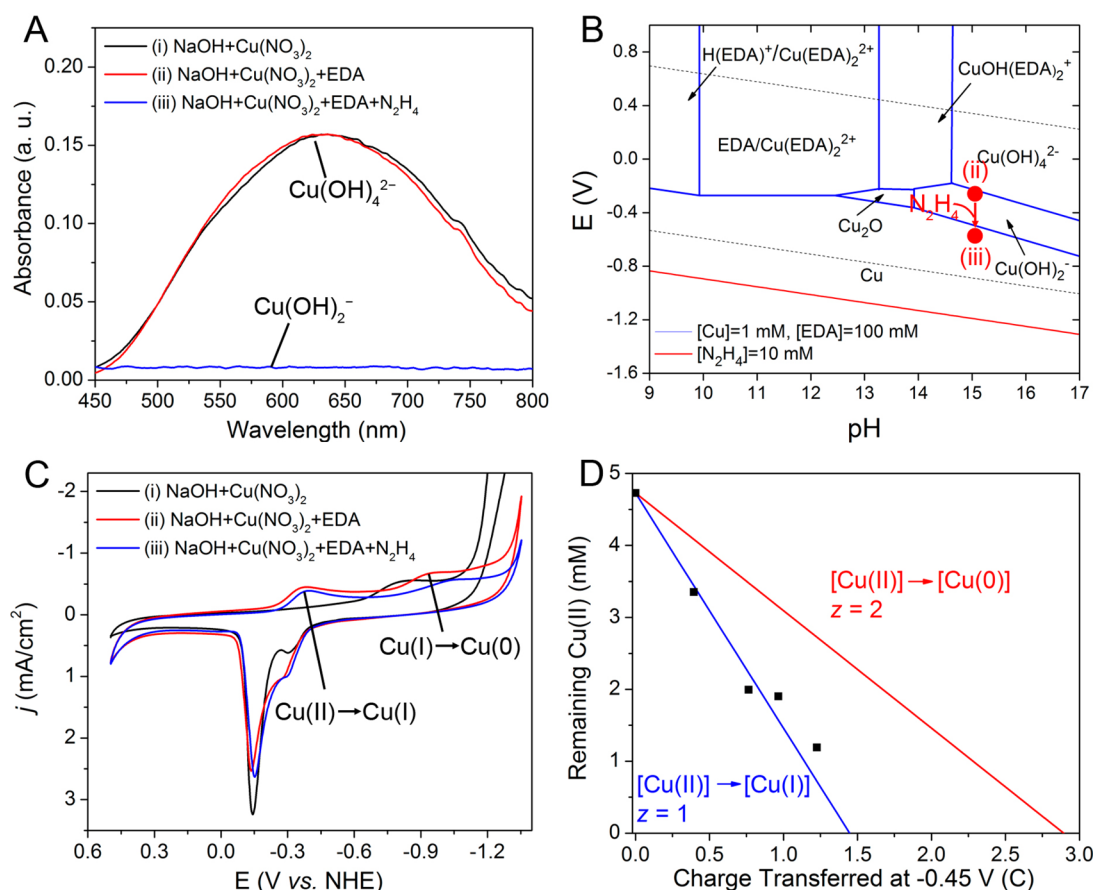


Figure 3. (A) UV-vis absorbance spectra of (i) 14.3 M NaOH + 4.7 mM $\text{Cu}(\text{NO}_3)_2$, (ii) solution (i) + 0.11 M EDA, and (iii) solution (ii) + 25 mM N_2H_4 . (B) Pourbaix diagram of the Cu-EDA- H_2O system with 1 mM of Cu(II) and 100 mM of EDA. (C) CVs of solutions i, ii, and iii at 100 mV s^{-1} . (D) Remaining $\text{Cu}(\text{OH})_4^{2-}$ vs charge transferred during the reduction of $\text{Cu}(\text{OH})_4^{2-}$ at -0.45 V. Straight lines represent the theoretical trend for a one- or two-electron reduction of $\text{Cu}(\text{OH})_4^{2-}$.

thermocouple was calibrated by comparing the output to a secondary thermocouple located in the cell under the same reaction conditions (Figure S1). By measuring the lengths of the Cu nanowires in different frames, we determined the growth rate of individual nanowires.

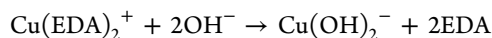
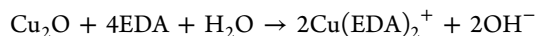
The growth of Cu nanowires was examined under various temperatures, concentrations of Cu ions ($[\text{Cu}(\text{II})]$), and concentrations of hydrazine ($[\text{N}_2\text{H}_4]$). As seen in Figure 2A, the axial growth rate of the Cu nanowires is constant over time; this was the case for all the experimental conditions for which we show data in Figure 2. When the reaction was carried out with $[\text{Cu}(\text{II})] = 4.7$ mM and $[\text{N}_2\text{H}_4] = 25$ mM at 343 K, the Cu nanowires grew at a rate (dL/dt , where L is the nanowire length and t is the growth time) of 86 ± 4 nm s^{-1} . If $[\text{Cu}(\text{II})]$ was increased from 1.9 to 5.6 mM while keeping $[\text{N}_2\text{H}_4]$ and temperature (T) constant, the growth rate increased linearly from 17 to 103 nm s^{-1} with a slope of 24 nm s^{-1} mM $^{-1}$ (Figure 2B). In contrast, the growth rate is independent of $[\text{N}_2\text{H}_4]$ between 19.8 and 62.6 mM (Figure 2C), indicating that the reduction of the ionic copper precursor is not the rate-limiting step responsible for nanowire growth. The growth rate is also temperature dependent, and increases with increasing temperature from 333 to 363 K (Figure 2D). The log of the growth rate is linear with respect to the reciprocal of the temperature with a slope of -600 nm K s^{-1} at $[\text{Cu}(\text{II})] = 4.7$ mM and $[\text{N}_2\text{H}_4] = 25$ mM. Cu nanowires do not form outside of the

range of concentrations and temperatures shown in Figure 2B–D.

To facilitate the further interpretation of this real-time growth data, we will first provide additional experimental results to show that the species adding to the Cu nanowires is $\text{Cu}(\text{OH})_2^-$. Prior to the addition of EDA and N_2H_4 , the solution of Cu(II) in concentrated NaOH (pH ~ 15) appears deep blue, with a broad absorption peak at ~ 650 nm (curve i, Figure 3A). This absorption spectrum is consistent with the formation of a $\text{Cu}(\text{OH})_4^{2-}$ complex.³⁹ After addition of EDA there is negligible change in the absorption spectrum (curve ii, Figure 3A). By titrating NaOH into a solution containing EDA and Cu(II), we can observe that there is no spectral difference between a solution of Cu(II) and NaOH with or without EDA at a $[\text{NaOH}] > 14.3$ M (Figure S2). These results indicate that EDA does not coordinate to Cu(II) under the conditions used for the Cu nanowire synthesis.

If N_2H_4 is added to the blue solution containing NaOH, EDA, and Cu(II), the solution turns colorless and the absorption peak disappears (curve iii, Figure 3A). This spectral change indicates that the colored $\text{Cu}(\text{OH})_4^{2-}$ complex has been reduced to a colorless Cu(I) complex. The color change is accompanied by the formation of N_2 bubbles from the oxidation of N_2H_4 . The Pourbaix diagram of the Cu-EDA- H_2O system indicates this Cu(I) species is $\text{Cu}(\text{OH})_2^-$ at pH = ~ 15 (Figure 3B, see the Supporting Information for the calculations). The clear reaction solution remains relatively

stable at room temperature, and neither Cu nanowires nor nanoparticles form for several hours. In contrast, rapid precipitation of Cu₂O octahedra occurs in the absence of EDA.³⁶ One possible explanation of this is that EDA enhanced the dissolution of Cu₂O nanoparticles to give Cu(EDA)₂⁺,⁴⁰ which is labile toward OH⁻ substitution:



EDA was also observed to stabilize Cu(OH)₂⁻ during cyclic voltammetry (CV). A cyclic voltammogram of Cu(II) in 14.3 M NaOH exhibits a broad reduction peak at ~ -0.8 V vs NHE, resulting in the deposition of Cu(0) on the electrode (curve i, Figure 3C). Because of the broad nature of the peak, it was difficult to determine if Cu(II) was reduced to Cu(0) directly or through a Cu(I) intermediate. In the reverse scan, sequential peaks corresponding to the oxidation of Cu(0) to Cu(I) and Cu(II) were observed. Upon addition of EDA, the broad reduction peak was split into two distinct peaks at -0.4 and -1.0 V (curve ii, Figure 3C). Upon further addition of N₂H₄ to the solution containing EDA, NaOH, and Cu(NO₃)₂, the CV profile exhibits no change (curve iii, Figure 3C).

In contrast to the second peak at -1.0 V that results in the heterogeneous deposition of Cu(0), the first peak at -0.4 V is a homogeneous process that arises from the reduction of Cu(OH)₄²⁻ to Cu(OH)₂⁻. By scanning the potential between 0.1 and -0.7 V to avoid overlap with the reduction to Cu(0) at -1.0 V, we observed well-defined reversible redox peaks for the Cu(OH)₄²⁻/Cu(OH)₂⁻ redox couple. The peak current density (*j_p*) was proportional to the square root of the scan rate (*v*^{1/2}), indicating a diffusion-controlled redox process (Figure S3). Sustained electrolysis at -0.45 V resulted in conversion of the solution color from deep blue (indicating the presence of Cu(OH)₄²⁻) to nearly clear (indicating the presence of Cu(OH)₂⁻). By correlating the amount of charge transferred at -0.45 V to the concentration of Cu(OH)₄²⁻ that remained in the solution (Figure S4), we confirmed that the reduction processes occurring at -0.4 V is a one-electron reduction process (Figure 3D), consistent with reduction of Cu(OH)₄²⁻ to Cu(OH)₂⁻.

Now that we have partly addressed the question of the species that adds to the Cu nanowire, we turn our attention to showing that the growth of Cu nanowires is limited by the rate of diffusion of Cu(OH)₂⁻ to the surface of the nanowire. After they sprout from the seeds, Cu nanowires grow with a relatively uniform diameter (which is always smaller than the diameter of the seed).³⁸ Within the range of growth conditions studied here, which encompass the range of conditions for which Cu nanowires formed, the diameters of the Cu nanowires appear almost constant (see Table S1). From over 300 measurements, the radius of the Cu nanowires grown in the reaction cell was determined to be 30.6 ± 6.0 nm. Each growing nanowire can thus be approximated as an ultramicroelectrode with a constant diameter and tip surface area (*A*). According to previous HRTEM characterization, the Cu nanowires have a pentagonal cross section.³⁶ With an average nanowire radius of *r* = 30.6 nm, the area at the end of the nanowire is *A* = 3.44*r*² = 3221 nm² (see Figure S5 and S6). The electrochemical potential of the nanowire electrode is fixed at the redox potential of N₂H₄, resulting in a constant potential for reduction of Cu(OH)₂⁻. According to Faraday's Law, the mass added (*m*) to the

nanowire tip is proportional to the amount of charge transferred (*Q*):

$$m = \frac{QM}{zF} = \frac{ItM}{zF} \quad (1)$$

where *I* is the current passed through the nanowire, *F* is the Faraday constant, *M* is the molar mass of copper, and *z* (equal to 1) is the number of electrons necessary to reduce Cu(OH)₂⁻ to Cu(0).

To see if the growth of Cu nanowires is limited by the rate of diffusion, we compare the growth rate of a nanowire to the diffusion-limited maximum growth rate. At an ultramicroelectrode, the diffusion-limited steady-state current derived from Fick's second law is given by⁴¹

$$I = \frac{zFA}{r}DC \quad (2)$$

where *C* is the concentration of Cu(OH)₂⁻, and *D* ≈ 0.91 × 10⁻⁶ cm² s⁻¹ is the diffusion coefficient for Cu(OH)₂⁻ at 343 K. We determined the diffusion coefficient for Cu(OH)₂⁻ from the slope of the plot of *j_p* vs *v*^{1/2} (Figure S3) and the Randles-Sevcik equation (Table S2):⁴²

$$j_p = 0.4463zFC \left(\frac{zFvD}{RT} \right)^{1/2} \quad (3)$$

where *R* is the gas constant. The diffusion coefficient obtained here is comparable to those of reported for other Cu complexes in the literature (Table S3).⁴³

By combining eq 2 and *dm* = 2.79*ρr*²*dL* with eq 1, the diffusion-limited rate of nanowire growth at a given temperature is

$$\frac{dL}{dt} = 1.23 \left(\frac{M}{\rho r} \right) DC \quad (4)$$

where *ρ* is the density of copper. With eq 4, the maximum growth rate of a nanowire is linearly dependent on [Cu(II)] with a slope of 26 nm s⁻¹ mM⁻¹ at 343 K. This is only slightly larger than the experimentally measured nanowire growth rate dependence on [Cu(II)] of 24 nm s⁻¹ mM⁻¹ at 343 K (Figure 2B). These data are very strong evidence in support of a model by which Cu nanowires grow through the diffusion limited addition of Cu(OH)₂⁻ to the end of the nanowire.

Additional evidence for the diffusion-controlled growth of Cu nanowires comes from the low activation energy, *E_a*, for nanowire growth. From eq 4 and *D* = *D*₀e^{-*E_a*/RT} (*D*₀ is the frequency factor), we can show that the log of the growth rate is linearly dependent on the reciprocal of temperature at fixed reagent concentrations:

$$\ln \left(\frac{dL}{dt} \right) = \frac{\left(-\frac{E_a}{R} \right)}{T} + \ln \left[1.23 \left(\frac{MC}{\rho r} \right) D_0 \right] \quad (5)$$

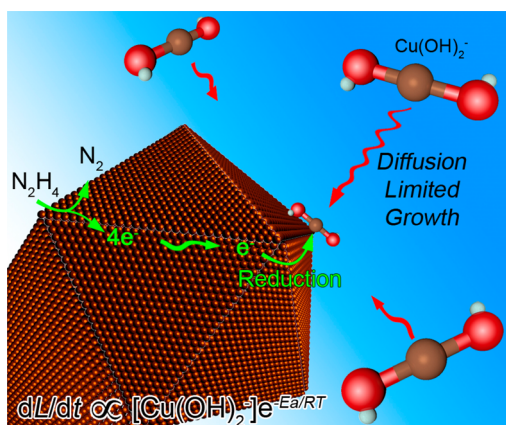
By fitting the data in Figure 2D with eq 5, we determined the activation energy for Cu nanowire growth to be 11.5 kJ mol⁻¹ (Table S4). Such a low value indicates a diffusion-controlled process.⁴⁴

Finally, we show that N₂H₄ provides the thermodynamic driving force for reduction of the Cu(OH)₂⁻ intermediate at elevated temperatures. We verified this by measuring the open circuit potential (OCP) in the growth solution with a Cu nanowire network on a glass substrate as the working electrode.⁴⁵⁻⁴⁷ An OCP of -0.30 V was measured in a

solution of Cu(II)/EDA/NaOH, a potential that stabilizes Cu(II) as indicated by the Pourbaix diagram (Figure 3B). Addition of N_2H_4 lowered the OCP to -0.62 V, a potential sufficient to reduce Cu(II) to Cu(I), but insufficient to further reduce Cu(I) to Cu(0) at room temperature. This is consistent with the observation that the clear reaction solution containing $Cu(OH)_2^-$ is stable at room temperature. However, elevating the solution temperature in the electrochemical cell to 343 K decreased the OCP to -0.70 V, suggesting that increasing the temperature increased the potential of N_2H_4 to give up its electrons to Cu(I). In addition, the increase in temperature shifted the onset potential of reduction of Cu(I) to Cu(0) from -0.75 to -0.68 V. These two effects together contribute to the reduction of $Cu(OH)_2^-$ to metallic copper at elevated temperatures.

We summarize the above results and analysis with the Cu nanowire growth model illustrated in Scheme 1. Oxidation of

Scheme 1. Growth Model of Cu Nanowires



N_2H_4 provides the electrochemical potential for reduction of Cu(I) to Cu(0) at the end of the nanowire at 343 K. Once this potential is in place, the growth rate is kinetically limited not by the concentration of the reducing agent, N_2H_4 , but by the diffusion of $Cu(OH)_2^-$ to the end of the nanowire.

In conclusion, we demonstrate the first diffusion-controlled model for nanowire growth in solution. We further provide spectroscopic and electrochemical data that suggest that Cu nanowires grow through the addition of $Cu(OH)_2^-$. As the nanowire growth does not depend on the concentration of the reducing agent, N_2H_4 , the role of this species is to provide the potential necessary to reduce $Cu(OH)_4^{2-}$ to $Cu(OH)_2^-$ at room temperature, and $Cu(OH)_2^-$ to Cu(0) at elevated temperatures. We now know what species adds to a growing copper nanowire, the rate limiting step of nanowire growth, and the activation energy for nanowire growth. From previous work, it is clear that EDA affects the growth rate and aspect ratio of copper nanowires,³⁸ but there is still no direct experimental evidence to verify why the nanowire grows in one dimension. Nevertheless, we expect this model of diffusion-controlled growth can be applied to better understand a wide variety of nanostructure syntheses, leading to better control over the assembly of atoms into well-defined morphologies with desirable properties.

■ ASSOCIATED CONTENT

Supporting Information

Detailed description of experimental methods, additional figures, and a movie showing real time growth of Cu nanowires. This material is available free of charge via the Internet at <http://pubs.acs.org>.

■ AUTHOR INFORMATION

Corresponding Author

*(B.J.W.) E-mail: Benjamin.wiley@duke.edu.

Author Contributions

[†]These authors contributed equally. The manuscript was written through contributions of all authors. All authors have given approval to the final version of the manuscript.

Notes

The authors declare no competing financial interests.

■ ACKNOWLEDGMENTS

This work was supported in part by the National Science Foundation's (NSF's) Research Triangle MRSEC (DMR-1121107), an NSF CAREER award (DMR-1253534), and NSF Grant No. ECCS-1344745. Y.-C.H. was supported by the research fund from KERI (No. 13-02-N0104-01).

■ REFERENCES

- (1) Whitesides, G. M.; Mathias, J. P.; Seto, C. T. *Science* **1991**, *254*, 1312.
- (2) Whitesides, G. M.; Grzybowski, B. *Science* **2002**, *295*, 2418.
- (3) Hu, J.; Odom, T. W.; Lieber, C. M. *Acc. Chem. Res.* **1999**, *32*, 435.
- (4) Rao, C. N. R.; Deepak, F. L.; Gundiah, G.; Govindaraj, A. *Prog. Solid State Chem.* **2003**, *31*, 5.
- (5) Xia, Y.; Yang, P.; Sun, Y.; Wu, Y.; Mayers, B.; Gates, B.; Yin, Y.; Kim, F.; Yan, H. *Adv. Mater.* **2003**, *15*, 353.
- (6) Law, M.; Goldberger, J.; Yang, P. *Annu. Rev. Mater. Res.* **2004**, *34*, 83.
- (7) Tang, Z.; Kotov, N. A. *Adv. Mater.* **2005**, *17*, 951.
- (8) Cademartiri, L.; Ozin, G. A. *Adv. Mater.* **2009**, *21*, 1013.
- (9) Repko, A.; Cademartiri, L. *Can. J. Chem.* **2012**, *90*, 1032.
- (10) Morales, A. M.; Lieber, C. M. *Science* **1998**, *279*, 208.
- (11) Kodambaka, S.; Tersoff, J.; Reuter, M. C.; Ross, F. M. *Science* **2007**, *316*, 729.
- (12) Ross, F. M. *Rep. Prog. Phys.* **2010**, *73*, 114501.
- (13) Tang, Z.; Kotov, N. A.; Giersig, M. *Science* **2002**, *297*, 237.
- (14) Koh, W.-K.; Bartnik, A. C.; Wise, F. W.; Murray, C. B. *J. Am. Chem. Soc.* **2010**, *132*, 3909.
- (15) Yuwono, V. M.; Burrows, N. D.; Soltis, J. A.; Penn, R. L. *J. Am. Chem. Soc.* **2010**, *132*, 2163.
- (16) Cademartiri, L.; Guerin, G.; Bishop, K. J. M.; Winnik, M. A.; Ozin, G. A. *J. Am. Chem. Soc.* **2012**, *134*, 9327.
- (17) <http://www.cambrios.com/>.
- (18) Leem, D.-S.; Edwards, A.; Faist, M.; Nelson, J.; Bradley, D. D. C.; de Mello, J. C. *Adv. Mater.* **2011**, *23*, 4371.
- (19) Yang, L.; Zhang, T.; Zhou, H.; Price, S. C.; Wiley, B. J.; You, W. *ACS Appl. Mater. Interfaces* **2011**, *3*, 4075.
- (20) Song, M.; You, D. S.; Lim, K.; Park, S.; Jung, S.; Kim, C. S.; Kim, D.-H.; Kim, D.-G.; Kim, J.-K.; Park, J.; Kang, Y.-C.; Heo, J.; Jin, S.-H.; Park, J. H.; Kang, J.-W. *Adv. Funct. Mater.* **2013**, *23*, 4177.
- (21) Kodambaka, S.; Tersoff, J.; Reuter, M. C.; Ross, F. M. *Phys. Rev. Lett.* **2006**, *96*, 096105.
- (22) Eswaramoorthy, S. K.; Howe, J. M.; Muralidharan, G. *Science* **2007**, *318*, 1437.
- (23) Dubrovskii, V. G.; Sibirev, N. V.; Harmand, J. C.; Glas, F. *Phys. Rev. B* **2008**, *78*, 235301.
- (24) Liao, H.-G.; Cui, L.; Whitelam, S.; Zheng, H. *Science* **2012**, *336*, 1011.

- (25) Wang, H.; Zepeda-Ruiz, L. A.; Gilmer, G. H.; Upmanyu, M. *Nat. Commun.* **2013**, *4*, 1956.
- (26) Stach, E. A.; Pauzauskie, P. J.; Kuykendall, T.; Goldberger, J.; He, R.; Yang, P. *Nano Lett.* **2003**, *3*, 867.
- (27) Zheng, H.; Smith, R. K.; Jun, Y.-W.; Kisielowski, C.; Dahmen, U.; Alivisatos, A. P. *Science* **2009**, *324*, 1309.
- (28) Sun, Y.; Wang, Y. *Nano Lett.* **2011**, *11*, 4386.
- (29) Li, D.; Nielsen, M. H.; Lee, J. R. I.; Frandsen, C.; Banfield, J. F.; De Yoreo, J. J. *Science* **2012**, *336*, 1014.
- (30) Sun, Y. *Mater. Today* **2012**, *15*, 140.
- (31) Yuk, J. M.; Park, J.; Ercius, P.; Kim, K.; Hellebusch, D. J.; Crommie, M. F.; Lee, J. Y.; Zettl, A.; Alivisatos, A. P. *Science* **2012**, *336*, 61.
- (32) Liao, H.-G.; Niu, K.; Zheng, H. *Chem. Commun.* **2013**, *49*, 11720.
- (33) Liao, H.-G.; Zheng, H. *J. Am. Chem. Soc.* **2013**, *135*, 5038.
- (34) Rathmell, A. R.; Bergin, S. M.; Hua, Y.-L.; Li, Z.-Y.; Wiley, B. J. *Adv. Mater.* **2010**, *22*, 3558.
- (35) Rathmell, A. R.; Nguyen, M.; Chi, M.; Wiley, B. J. *Nano Lett.* **2012**, *12*, 3193.
- (36) Ye, S.; Rathmell, A. R.; Ha, Y.-C.; Wilson, A. R.; Wiley, B. J. *Small* **2014**, *10*, 1771.
- (37) Sun, Y.; Mayers, B.; Herricks, T.; Xia, Y. *Nano Lett.* **2003**, *3*, 955.
- (38) Ye, S.; Rathmell, A. R.; Stewart, I. E.; Ha, Y.-C.; Wilson, A. R.; Chen, Z.; Wiley, B. J. *Chem. Commun.* **2014**, *50*, 2562.
- (39) Chao, Y.-Y. H.; Kearns, D. R. *J. Phys. Chem.* **1977**, *81*, 666.
- (40) Aksu, S.; Doyle, F. M. *J. Electrochem. Soc.* **2002**, *149*, B340.
- (41) Bard, A. J.; Faulkner, L. R. *Electrochemical Methods: Fundamentals and Applications*, 2nd ed.; John Wiley & Sons, Inc.: New York, 2001.
- (42) Zanello, P. *Inorganic Electrochemistry: Theory, Practice and Application*; The Royal Society of Chemistry: London, 2003.
- (43) Norkus, E. *J. Appl. Electrochem.* **2000**, *30*, 1163.
- (44) Bamford, C. H.; Tipper, C. F. H.; Compton, R. G. in *Comprehensive Chemical Kinetics: Diffusion-Limited Reactions*; Elsevier: Amsterdam, 1985; Vol. 25.
- (45) Chen, Z.; Rathmell, A. R.; Ye, S.; Wilson, A. R.; Wiley, B. J. *Angew. Chem., Int. Ed.* **2013**, *52*, 13708.
- (46) Chen, Z.; Ye, S.; Wilson, A. R.; Ha, Y.-C.; Wiley, B. J. *Energy Environ. Sci.* **2014**, *7*, 1461.
- (47) Rathmell, A. R.; Wiley, B. J. *Adv. Mater.* **2011**, *23*, 4798.